# Assessment of commercial software for simulation of chaotic electrokinetic phenomena

**By E. Karatay, C. L. Druzgalski AND A. Mani**

## 1. Motivation and objectives

The investigation of non-equilibrium electric double layer (EDL) physics is essential for both applied and fundamental aspects of electrokinetic phenomena near charge-selective surfaces such as ion exchange membranes and particles, electrodes and micro/nanochannel intersections. (Mishchuk 2010) EDL physics and the associated phenomena are critical for electric field-driven transport through ion-selective media in electrolyte solutions. Hence EDL physics is of interest in various research fields and has a wide span of applications ranging from conventional electrodialysis for water purification (Nikonenko *et al.* 2014) to micro/nanofluidic separations (Zangle *et al.* 2010; Green *et al.* 2014). Previous experimental (e.g. Kwak *et al.* 2013; Fleury *et al.* 1992), numerical (e.g. Manzanares *et al.* 1993; Rubinstein & Zaltzman 2000) and theoretical (e.g. Rubinstein & Zaltzman 2001; Yariv 2009; Bazant & Squires 2004) reports indicate that such applications involve chaotic transport phenomena that arise due to electroosmotic instabilities (EOI) stemming from the coupling of hydrodynamics with ion transport and electrostatic forces.

Theoretical and numerical investigations of EOI often employed either one-dimensional models (Manzanares *et al.* 1993) and methods of matched asymptotics (Chu & Bazant 2005) under-predicting the experimentally measured ion-fluxes (Matsuura *et al.* 2013; Krol 1999) or an effective slip approximation by assuming the quasi-steadiness of the extended space charge (ESC) layer (Rubinstein & Zaltzman 2000) where the EOI flow has been predicted as arrays of steady vortex pairs. Recently, there have been a few two-dimensional direct numerical simulations (DNS) of EOI solving the fully coupled Poisson-Nernst-Planck and Navier-Stokes equations (Demekhin *et al.* 2011, 2013; Druzgalski *et al.* 2013; Davidson *et al.* 2014). Druzgalski *et al.* (2013) and Demekhin *et al.* (2013) have reported electrokinetic instability and transition to chaotic flows beyond a threshold value of applied electric potential, $\sim \mathcal{O}(1)$ V. Transitions from regular coherent vortex pairs to chaotic multi-scale vortex structures have been reported at strong electric forcing. These recent investigations have revealed the presence of a wide range of spatio-temporal scales in such chaotic systems similar to those observed in turbulent flows. To best describe and well resolve the chaotic multi-scale structures encountered at high electric forcing, efficient DNS codes specifically developed for capturing the overlimiting conductance physics are of high importance for accurate predictions at reasonable computational cost. Previous reports on DNS of electrokinetic chaos have employed custom-made codes tailored to the specific physics (Druzgalski *et al.* 2013; Demekhin *et al.* 2011, 2013; Davidson *et al.* 2014). However, there has been no investigation of the efficiency of general-purpose commercial computational fluid dynamics (CFD) software for the prediction of electrokinetic chaos stimulated by electroosmotic instabilities.

General-purpose commercial CFD software can be attractive due to their easy-to-use-environment, providing integrated packages for mesh generation in complex geometries,

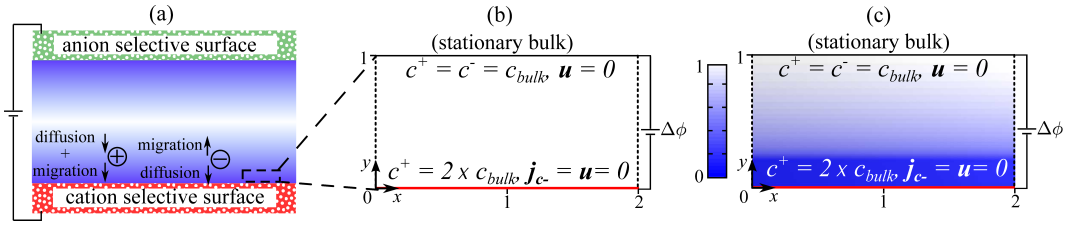


FIGURE 1. Model problem and computational domain. a) Schematic plot of stationary salt concentration distribution in between anion and cation selective surfaces. b) Computational domain with an aspect ratio of 2. c) Stationary anion concentration $c^-$ profile obtained from steady calculations. Here $\Delta\phi = 3\ V$. Color bar shows dimensionless $c^-$ variation.

various built-in solvers applicable to a broad range of physical systems governed by PDEs and post-processing visualization tools. However, to ensure numerical robustness, such software often employ numerical algorithms that tend to smooth fields in the space-time domain. Examples of such methods include, spatial discretization of fluxes via upwind, or TVD methods, and time integration via global implicit solvers. These methods are appropriate for systems that are inherently smooth, such as laminar flows, and heat transfer problems. They are also appropriate for turbulence closure models, since they aim to capture only the smooth time-averaged fields and not the violent instantaneous picture.

Chaotic systems, however, by nature compete against smoothness, and the question remains whether numerical smoothing can impose a conflicting constraint when a commercial software is used for simulation of such systems. The answer to this question depends on the specific physical problem, and there have been been several attempts in the literature to study the performance of commercial CFD codes in both laminar and turbulent flows for various applications (Iaccarino 2001; Freitas 1995; Tucker 1997; Glatzel *et al.* 2008). Previous reports indicate that detailed comparative analyses are crucial when simulating complex flows, where a wide range of spatio-temporal scales are involved (Iaccarino 2001; Mittal & Moin 1997). In the context of turbulent flows, flow over a cylinder is one of the most extensively studied yet challenging turbulent flow exhibiting various regimes with different modes of instabilities (Beaudan & Moin 1994; Kravchenko & Moin 2000; Mittal & Moin 1997; Catalano *et al.* 2003; Breuer 1998). Comparisons of the detailed turbulent statistics have indicated the notorious impact of numerical dissipation on high wave number fluctuations (Mittal & Moin 1997).

In this report, we consider transient DNS of the coupled Poisson-Nernst-Planck (PNP) and Navier-Stokes (NS) equations in 2D using a commercial general-purpose CFD package. Among various commercial solver alternatives, we have chosen Comsol Multiphysics because it is frequently employed in the relevant research fields (e.g. membrane science, microfluidics, and electrochemistry) where the effects of non-equilibrium EDL physics can be crucial. We study the efficiency of Comsol Multiphysics for the prediction of chaotic electrokinetic phenomena for the first time. We compare the accuracy and efficiency of a Comsol-based DNS code against a verified custom-made DNS code tailored to resolve the chaotic electrokinetic phenomena. We compare the detailed statistics including broadband energy and concentration spectra calculated from the results obtained by both Comsol-based and custom-made DNS codes.

## 2. Model problem

Figure 1(a) shows a system consisting of a stationary electrolyte solution in between an anion selective surface and a cation selective surface, e.g. anion and cation exchange membranes, respectively. Once an electric field is applied across this system, concentration gradients establish, leading to salt depletion near ion selective surfaces. Schematically depicted in Figure 1(a) is the one-dimensional stationary transport at low voltages while the bulk of the solution is still stationary. Here, we consider a small section of this system adjacent to the cation selective surface (Figure 1(a-b)). Choosing such a small domain reduces our model problem to a representative system of an initially stationary salt solution in between a cation selective surface and a stationary homogeneous bulk, as in Druzgalski *et al.* (2013). Our computational domain is periodic in the tangential direction $x-$ with an aspect ratio of 2 (Figure 1(b)). For a fair comparison of the commercial and the custom-made DNS codes, we consider this small system which can be simulated by a single core, excluding the potential effects of parallelization efficiency of the codes.

### 2.1. *Governing equations*

We solve for the electric potential distribution, ion, and momentum transport for a dilute solution of a monovalent symmetric strong salt. Incompressible Navier-Stokes and Poisson-Nernst-Planck equations describe the flow, ion distribution, and electric potential, respectively.

$$0 = -\boldsymbol{\nabla} p + \mu \boldsymbol{\nabla^2 u} + \rho_e \boldsymbol{E}, \tag{2.1a}$$

$$\boldsymbol{\nabla} \cdot \boldsymbol{u} = 0, \tag{2.1b}$$

$$\frac{\partial c^{\pm}}{\partial t} = -\boldsymbol{\nabla} \cdot (c^{\pm} \boldsymbol{u} - D \boldsymbol{\nabla} c^{\pm} \pm D V_T^{-1} c^{\pm} \boldsymbol{\nabla} \phi), \tag{2.1c}$$

$$-\varepsilon \boldsymbol{\nabla^2} \phi = \rho_e, \tag{2.1d}$$

where $\boldsymbol{u} = u\boldsymbol{x} + v\boldsymbol{y}$ is the velocity vector field; $p$, $c^+$, $c^-$, and $\phi$ are hydrodynamic pressure, cation concentration, anion concentration, and electric potential, respectively. Here $\boldsymbol{E} = -\boldsymbol{\nabla}\phi$ is electric field, and $\rho_e$ is the free charge density given by $e(c^+ - c^-)$ for a monovalent symmetric salt; $\mu$, $D$, and $\varepsilon$ are the viscosity, diffusion coefficient of ions and dielectric permittivity of the fluid, respectively. Moreover, $V_T = k_B T/e$ is the thermal voltage where $k_B$ and $e$ are the Boltzmann constant and elementary charge, respectively.

Eqs. (2.1*a*)-(2.1*d*) are solved in 2D with the boundary conditions demonstrated in Figure 1(b-c). Here the spatial coordinates are scaled by the surface-to-bulk distance $L$. On the cation selective surface at y=0, there is no slip, $\boldsymbol{u} = 0$, and the potential is grounded, $\phi = 0$. We implement the ion selectivity at y=0 by enforcing a no-flux condition for anions, $\boldsymbol{j_{c^-}} = 0$, and a fixed cation concentration twice that of the bulk concentration, $c^+ = 2 \times c_{bulk}$. On the upper boundary at y=1, which is representative of a stationary homogeneous bulk solution, there is no slip, $\boldsymbol{u} = 0$, and the concentrations of both anions and cations are equal to the bulk salt concentration, $c^+ = c^- = c_{bulk}$. We implement the applied voltage $\phi = \Delta\phi$ at $y = 1$. We employ periodic boundary conditions for all variables between the boundaries x=0 and x=2.

### 2.2. *Key dimensionless parameters*

The key dimensionless parameters of our model problem are the $(i)$ electrohydrodynamic coupling constant $\kappa = \varepsilon V_T^2/(\mu D)$ $(ii)$ dimensionless Debye screening length $\epsilon = \lambda_D/L$ where $\lambda_D = \sqrt{\varepsilon k_B T/[2(ze)^2 c_{bulk}]}$ is the dimensional Debye length and $L$ is the domain

size in transverse direction y-, (*iii*) dimensionless applied potential $\Delta\phi/V_T$. The employed electrohydrodynamic coupling constant $\kappa$ corresponds to a typical value of 0.5 for dilute aqueous salt solutions. We consider a dimensionless Debye length $\epsilon$ of $10^{-3}$ representative of e.g. salt solution with $c_{bulk} = 1$ mM in a $L = 10$ $\mu$m gap. In this paper aiming at a comparative study of electrokinetic chaos solved by commercial and custom-made DNS, we perform simulations at a fixed dimensionless applied voltage of $120V_T$, i.e. 3 $V$, which is reported to be well above the onset of the chaotic regime ($\geq 40V_T$) in Druzgalski *et al.* (2013).

## 3. Numerical methods

We first solve the steady Poisson-Nernst-Planck equations (2.1*c*-2.1*d*) without the flow. Shown in Figure 1(c) is the resultant steady anion concentration field, corresponding to the traditional steady description of EDL and ESC. Then the initial condition for the transient calculations is generated by applying locally 1% of random perturbation to the anion and cation concentration fields obtained from the steady calculation. The dimensionless time step used for all calculations is $10^{-6}$ scaled by diffusion time $t_{diff} = L^2/D$. All the simulations are performed on Intel Xeon eight E5620 CPUs using a single CPU.

For a fair comparison between the two codes, an effort has been made to eliminate the uncertainties that can be associated with the computational grid, implementation of boundary conditions, and solution methodology. For example, a cartesian grid with the same stretching function in $y-$ has been used. We match the computational grids by means of either the number of mesh points or the number of degrees of freedom solved for.

### 3.1. *Commercial CFD code*

A graphical user interface (GUI) based mathematics module allowing for implementation of user-defined transport equations is used. The concentration fields (2.1*c*) are implemented in general PDE form. The potential distribution (2.1*d*) is implemented in pre-defined Poisson's Equation. All the scalar fields are solved using quadratic Lagrange interpolation functions for space discretization. No smoothing of boundary fluxes is allowed. Navier-Stokes and continuity equations (2.1*a*-2.1*b*) are implemented in weak formulation. Quadratic Lagrange shape functions are used for NS equations, whereas linear order was used for the continuity equation.

The steady solution of scalar fields at 120 $V_T$ are obtained using a built-in direct solver, multifrontal massively parallel sparse direct solver (MUMPS), with an auxiliary sweep of applied voltage with a minimum step of 1 $V_T$. For the transient calculations, a segregated solver is used where the flow and pressure are solved in the first segregated step followed by the second step for concentrations and potential at each time step. For both steps the direct MUMPS solver is employed. Different time-stepping methods are employed for comparison purposes. First, a time-discrete solver is used with two time-discrete levels employing second-order implicit backward differentiation. (Comsol 2013) Second, a Generalized-$\alpha$ method is used. Generalized-$\alpha$ is an implicit, second-order accurate method with a parameter $\alpha$ ($0 \leq \alpha \leq 1$) to control the damping of high frequencies, where numerical damping is more for smaller $\alpha$ (Comsol 2013). Several values of $\alpha$ ($= 0.1, 0.4, 0.8$ and $0.99$) are employed to study the effect of numerical dissipation on the prediction of chaotic transport.

Though unstructured grids can be used in FEM based Comsol, the simulations were

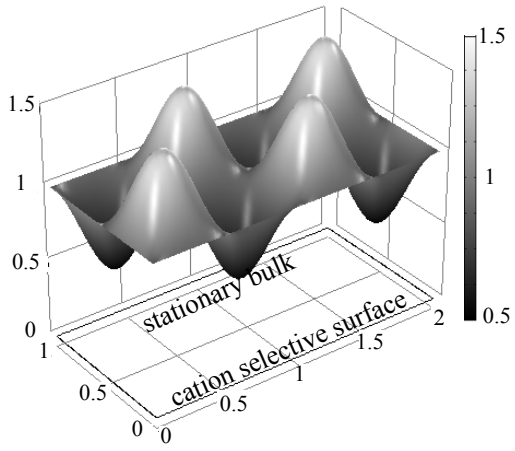


FIGURE 2. Manufactured solution for anion concentration field $c^-$.

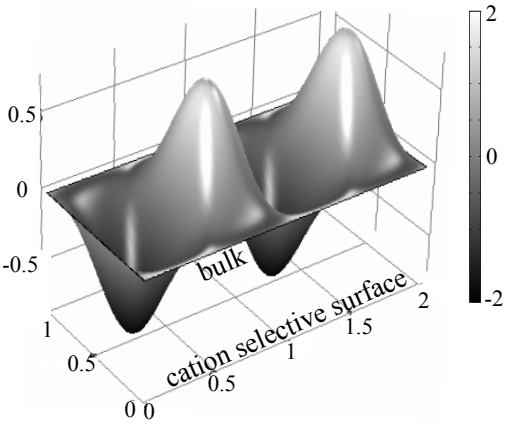


FIGURE 3. Manufactured solution for wall-normal velocity $v$ field.

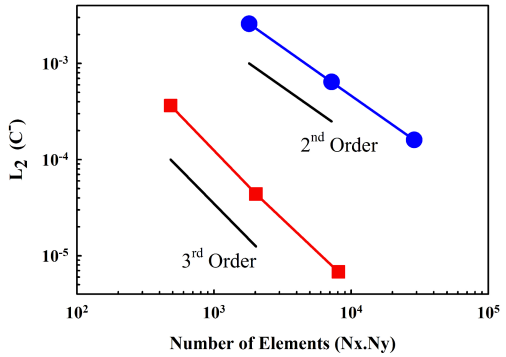


FIGURE 4. $L_2$-error estimates of dimensionless anion concentration $c^-/c_{bulk}$ calculated by the 2D manufactured solution with respect to spatial grid refinement. Red squares represent Comsol results. Blue circles represent reference custom-made DNS results.

performed on the same structured grid as in the custom-based DNS code with different resolutions to confirm the mesh independency of the solution in the vicinity of the membrane boundary. The scaled y-direction length is 1 with $N_y$ mesh points, and the scaled x-direction width is 2 with $N_x$ mesh points. With the considerations of fourth-order interpolation functions, we present results for two mesh resolutions. First, the number of grid points and second, the number of degrees of freedom (DOF) are matched with the mesh used in the custom-based DNS calculations.

### 3.2. *Custom-made DNS code*

We employ the same custom-made DNS code as in our previous work (Druzgalski *et al.* 2013), presenting a comprehensive analyses on instability and chaos in dilute electrolyte solutions near ion selective surfaces. Here we use the same computational details. In brief, transport in the periodic x- direction is treated with explicit second-order central finite-difference schemes. In the wall-normal y- direction, advection terms are treated explicitly, whereas the electromigration and diffusion terms are treated implicitly due to

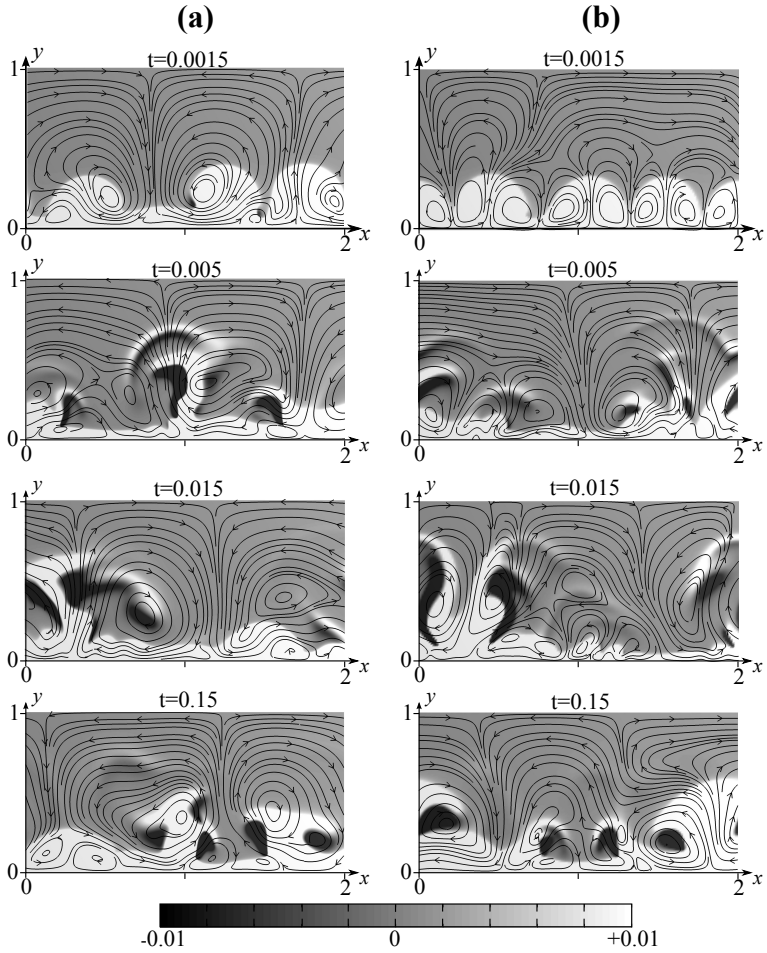


FIGURE 5. Comparison of instantaneous contour plots of dimensionless anion concentration field $c^-/c_{bulk}$ superimposed with flow lines a) obtained from custom-made DNS code, b) obtained by commercial Comsol Multiphysics code. Here $\Delta\phi = 120V_T$, and time is scaled by diffusion time $L^2/D$. The DOF solved for in both codes are matched by proper selection of grid resolution.

the numerical stiffness associated with the quasi-steady EDL. Potential, pressure, and the velocity fields are solved at each time step using a direct solver utilizing Fourier transforms in the x-direction and banded matrices in the y-direction. A semi-implicit scheme is used for time integration of the ionic concentration fields.

## 4. Results

The accuracy of both commercial and custom-made codes has been verified using the method of manufactured solutions (MMS) against a class of exact solutions (Kambiz & Patrick 2000). These exact solutions are smooth functions constructed to our set of governing equations modified with forcing source terms. Figures 2 and 3 reveal representative manufactured solutions for the anion concentration field $c^-(x, y, t)$ and wall-normal velocity field $v$, respectively. The maximum error ($L_\infty$-error) and area-averaged error ($L_2$-error) for velocity field $\boldsymbol{u}(x, y, t)$ and anion concentration $c^-(x, y, t)$ are calculated.

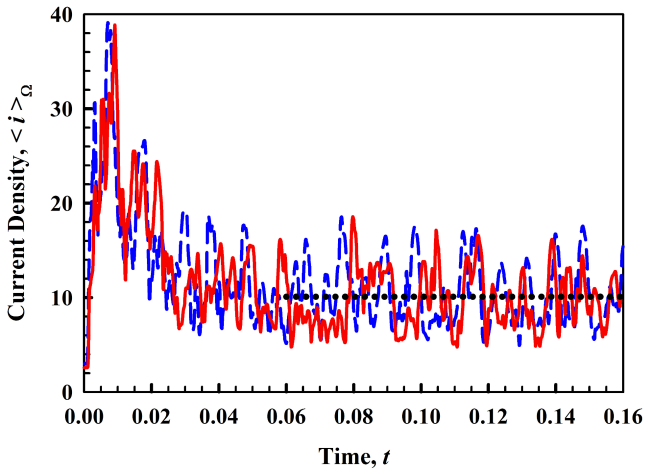


FIGURE 6. Space-averaged current density through the ion-selective surface, calculated at an applied potentional of $\Delta\phi = 3V$ from the results solved by custom-made DNS (blue dash line, ▬ ▬ ) and Comsol-based DNS codes (red solid line, ▬▬ ). Horizontal black dotted line depicts the time- and space-averaged current density evaluated from $t = 0.06$ to $t = 0.16$.

Third-order convergence is obtained for Comsol (Figure 4). Our MMS analysis indicates the accuracy of Comsol with proper mesh resolution.

Figure 5 shows instantaneous snapshots of the evolution of free charge density $\rho_e = (c^+ - c^-)/c_{bulk}$ with superimposed flow streamlines obtained from custom-based DNS (Figure 5(a)) and Comsol-based DNS (Figure 5(b)). In these simulations we match the number of degrees of freedom by employing a mesh with $N_x = 320$ and $N_y = 180$ in the custom-based DNS and $N_x = 170$ and $N_y = 95$ in the Comsol-based DNS. To minimize the potential effects of numerical dissipation on Comsol results, we employ a maximal value of parameter $\alpha = 0.99$ in the Generalized-$\alpha$ solver settings. We qualitatively compare the time evolution of electrohydrodynamic instability.

At very early times ($< 0.0015$), the anion concentration field has a diffusive nature (as in Figure 1(c)) and ESC is quasi-steady with a positive net free charge. However, instability starts to develop in time, leading to distortions in the quiescent structure of ESC (Figure 5(a-b) at $t$=0.0015). As the flow streamlines indicate, high concentration fluid ($\approx 1$) is advected towards the ion-selective surface, and low concentration fluid ($\approx 0$) is advected towards the bulk of the solution. At intermediate times (second and third panels in Figure 5), the instability and strength of the vortices grow in time. In addition, patches of negative charge emerge from the initially positive free charge $\rho_e$ layer adjacent to the ion-selective boundary and advected by the dynamic vortices further towards the bulk. At a long enough time (here shown at $t$=0.15), instability is fully developed. Both the custom-made and Comsol-based simulations predict strong spatio-temporal variations in concentration and flow fields indicative of the chaotic nature of the electrokinetic phenomena studied at $\Delta\phi = 3V$. Our observations reveal that the results obtained from both codes are in qualitative agreement as well as consistent with previous findings (Druzgalski *et al.* 2013; Davidson *et al.* 2014).

Current density is given as $\boldsymbol{i}(x, y, t) = \boldsymbol{j_{c^+}} - \boldsymbol{j_{c^-}}$, where $\boldsymbol{j_{c^+}}$ and $\boldsymbol{j_{c^-}}$ are ion fluxes of cations and anions, respectively, driven by advection, diffusion, and migration. Therefore, these are described as $\boldsymbol{j_{c^\pm}} = c^\pm \boldsymbol{u} - D\boldsymbol{\nabla} c^\pm \pm DV_T^{-1} c^\pm \boldsymbol{\nabla}\phi$. We calculate the space-averaged current density $< \boldsymbol{i} >_\Omega (t)$ as well as both time- and space-averaged current density $\boldsymbol{I}$.

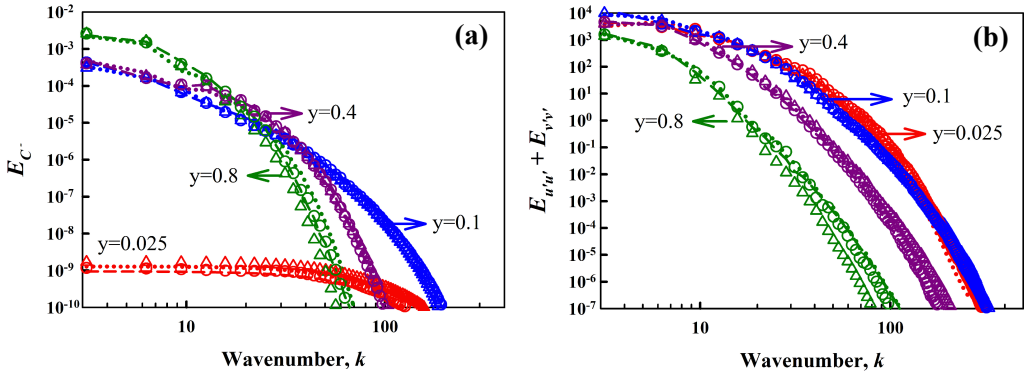


FIGURE 7. Broadband spatial spectrum of anion concentration $c^-$ (a) and kinetic energy (b) at different mesh resolutions with matched number of DOF solved by custom-based DNS and Comsol-based DNS. Symbols represent custom-made code results for coarser mesh with $N_x = 320$ and $N_y = 180$ (open triangles $\triangle$) and for finer mesh with $N_x = 600$ and $N_y = 340$ (open circles $\bigcirc$). Lines represent Comsol results for coarser mesh with $N_x = 170$ and $N_y = 95$ (dotted lines $\cdots$) and for finer mesh with $N_x = 320$ and $N_y = 180$ (dashed lines $-\,-$). Here Generalized-$\alpha$ time stepping is used with $\alpha = 0.8$ in Comsol simulations. Colors show the wall-normal distance which is also indicated by arrows both in (a) and (b). Red: $y = 0.025$, blue: $y = 0.1$, purple: $y = 0.4$, green: $y = 0.8$.

Figure 6 presents highly oscillatory space-averaged current density $< \boldsymbol{i} >_\Omega$ behavior obtained from the simulations shown in Figure 5(a-b). Both custom-made and Comsol-based DNSs predict a transient current until $t \approx 0.05$, at which time a statistically stationary, yet chaotic, state has been reached. Consistent with our findings, at sufficiently high electric forcing, fluctuations in the transient electric response of electrokinetic systems, either current density or voltage drop, have been also predicted by recent 2D simulations (Druzgalski *et al.* 2013; Demekhin *et al.* 2013; Rubinstein & Zaltzman 2000) and observed in experiments (Nikonenko *et al.* 2014). The black dot line in Figure 6 depicts the time- and space-averaged current density calculated for $0.06 < t < 0.16$ in the statistically stationary state, predicted to be the same in both codes.

To best present the wide range of length scales and the most distinct chaotic features in the current model problem, we compute one-dimensional spatial spectral density of anion concentration $c^-$ and velocity $\boldsymbol{u}$ in the homogenous direction. We plot spatial spectra of anion concentration $c^-$ (Figure 7(a)) and kinetic energy (Figure 7(b)) in x- direction at fixed wall-normal distances y=0.025, 0.1, 0.4, and 0.8. Comsol-based DNS predicts broadband structure of both quantities confirmative of chaotic transport as well as in agreement with the current custom-made DNS and previous reports (Druzgalski *et al.* 2013; Davidson *et al.* 2014). Note here that there is no inertial range in the spectra due to low Reynolds number and the chaotic flow is sustained without the need for inertia as unlike traditional turbulent flows.

At close proximity to the ion-selective boundary where the hydrodynamic instability grows, the anion concentration can have very small values (depleted zones) and can reveal sharp gradients both laterally and transversely (Figure 5). Grid convergence near y=0 is critical to resolve the EDL and the highly irregular ESC layer. The spatial spectra of concentration (Figure 7(a)) and energy (Figure 7(a)) calculated at y=0.025 reveal that the simulations are mesh-resolved, though slight variations are observed in the concentration spectra. At intermediate wall-normal distance y=0.4 and y=0.8, spatial spectra of both concentration and energy are well converged at both mesh resolutions. Furthermore, the

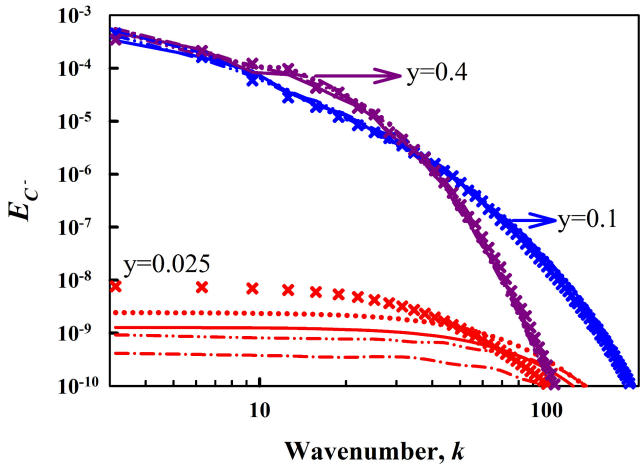


FIGURE 8. Effect of numerical dissipation and time-discretization method on one-dimensional anion concentration spectra. Symbols represent the time-discrete method and lines represent the Generalized-$\alpha$ method with different numerical damping. $\alpha = 0.99$ dotted lines ($\cdots$), $\alpha = 0.8$ solid lines (—), $\alpha = 0.4$ dash-dot-dot lines (—··), $\alpha = 0.99$ dash-dot lines (—·). Colors show the wall-normal distance which is also indicated by arrows, red: $y = 0.025$, blue: $y = 0.1$, purple: $y = 0.4$.

spectral densities calculated from both codes overlap in the full range of wavenumbers at intermediate y, clearly showing the good quantitative agreement between the two codes at the presented settings. However, our spectral analysis shows grid sensitivity even at a location further from y=0. As seen in Figure 7(b), at a wall-normal distance close to bulk y=0.8 where the y- grid spacing was chosen such that mesh resolution has affected a wide range of wavenumbers in the energy spectra calculated from custom-made DNS code utilizing non-dissipative second-order schemes.

Considering the fact that stability is often ensured by the addition of numerical dissipation in general purpose CFD software, we study the impact of numerical dissipation in temporal discretization. We control the numerical damping by varying the $\alpha$ parameter ($0 \leq \alpha \leq 1$) in the Generalized-$\alpha$ time-stepping method; several values of $\alpha$ are employed ($= 0.1, 0.4, 0.8, 0.99$) inducing more damping for smaller values of $\alpha$.

Figure 8 shows one-dimensional anion concentration spectra at selected y-positions obtained at different numerical damping implemented via the employed temporal discretization scheme. At intermediate y ($= 0.1$ and $= 0.4$), the same anion concentration distribution has been predicted for the entire wavenumber range irrespective of $\alpha$. However, the results are highly sensitive to numerical damping for all wavenumbers in the vicinity of the ion-selective boundary where the anion concentrations are very small due to ion depletion. Moreover, the smaller scale structures ($k_x > 120$) are damped for smaller $\alpha$. Furthermore, the predicted mean anion concentration at y=0.025, obtained by the integration of the shown spectra in Figure 8, is severely affected by numerical damping. $\alpha = 0.1$ estimates the mean anion concentration at y=0.025 to be $\sim 79\%$ lower than that obtained when $\alpha = 0.99$, providing minimal damping. Consistently for a fixed number of DOF, maximal damping with $\alpha = 0.1$ predicts $\sim 76\%$ lower mean anion concentrations compared to those obtained by the non-dissipative custom-made DNS code. These variations in the detailed statistics are reflected in the predicted global current density $\boldsymbol{I}$. Numerical damping of $\alpha = 0.1$ results in $\sim 5\%$ less current density $\boldsymbol{I}$ compared to

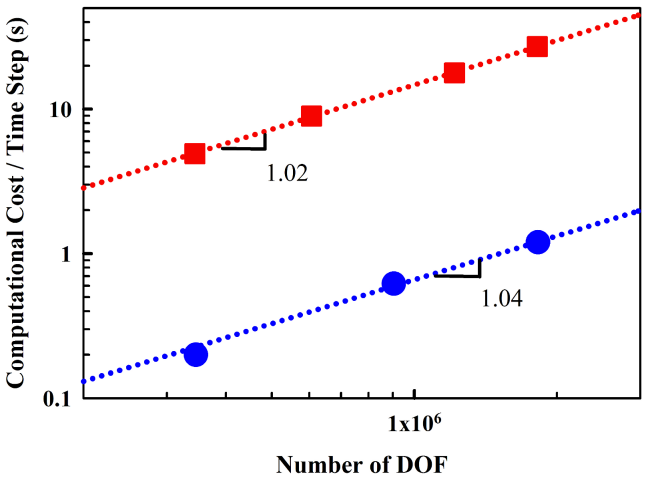


FIGURE 9. CPU time per time step required by Comsol-based code (red squares) and by custom-made code (blue circles) with respect to the number of degrees of freedom solved for. Dotted lines reveal linear regression with the slopes depicted.

that obtained by Comsol-based simulation with minimal damping of $\alpha = 0.99$ and by the simulation based on finite-difference schemes.

Among the readily built-in time-stepping methods provided by Comsol Multiphysics, we present results obtained by time-discrete method utilizing second-order BDF in comparison to those by the Generalized-$\alpha$ method (Figure 8). Our results are indicative of the sensitivity of detailed statistics to the employed time-stepping algorithm.

To further assess the performance of the employed commercial solver, we compare the CPU-time required to solve per time step by the Comsol-based DNS and the custom-made DNS codes. Almost a linear increase in computational cost is obtained for both codes with respect to increase in mesh resolution. However, the Comsol code is at least 20 times slower than the custom-made code developed specifically for predicting electrokinetic chaos. This is because the Comsol-based code handles all the terms implicitly, whereas the custom-made code utilizes both directional and term-specific semi-implicit discretization schemes.

## 5. Conclusions

We have investigated the performance of a general-purpose commercial CFD software, Comsol Multiphysics, on the 2D direct numerical simulations of transient chaotic electrokinetic phenomena, focusing on the accuracy, stability, and efficiency. As a benchmark analysis, we compared the results with those obtained by a central difference scheme-based custom code tailored to resolve chaotic electrokinetic phenomena. Accuracy is guaranteed with the proper selection of mesh resolution. High-order statistics revealed sensitivity towards numerical damping in temporal discretization in the vicinity of the ion-selective boundary. Low-order statistics and global current density have been affected by 5% with the addition of numerical damping. The results predicted by the commercial solver are in good quantitative agreement with those obtained by custom DNS; however, the commercial solver involves computational expense that is at least 20 times higher. Note that the computational domain in this study has been chosen small enough that

a single core is sufficient for the simulations with a reasonable solution time. We have resolved a small domain in close proximity to a cation-selective surface. Realistic systems require resolving much larger domains and often include several stacks of anion-selective and cation-selective surfaces, such as the processes in desalination and electrodialysis-based industries. Besides, our comparative results are in 2D, but the effects of three-dimensionality and confinement can be crucial in industrial systems. Therefore, parallel computing is essential for reducing the computational cost of simulations aimed at industrial applications. This impels the necessity of further investigations on the parallelization efficiency of the commercial software.

## Acknowledgments

The authors gratefully acknowledge helpful comments from Scott Davidson. The authors acknowledge the financial support provided by Netherlands Scientific Organization NWO through Rubicon grant.

## REFERENCES

Bazant, M. & Squires, T. 2004 Induced-charge electrokinetic phenomena: theory and microfluidic applications. *Phys. Rev. Lett.* **92**, 066101.

Beaudan, P. & Moin, P. 1994 *Numerical experiments on the flow past a circular cylinder at sub-critical reynolds number.* Technical Report no. TF-62, Department of Mechanical Engineering, Stanford University.

Breuer, M. 1998 Numerical and modeling influences on large eddy simulations for the flow past a circular cylinder. *Int. J. Heat Fluid Fl.* **19**, 512–521.

Catalano, P., Wang, M., Iaccarino, G. & Moin, P. 2003 Numerical simulation of the flow around a circular cylinder at high Reynolds numbers. *Int. J. Heat Fluid. Fl.* **24**, 463–469.

Chu, K. T. & Bazant, M. Z. 2005 Electrochemical Thin Films at and above the Classical Limiting Current. *SIAM J. App. Math* **65**, 1485–1505.

Comsol 2013 *Comsol Multiphysics Reference Manual for Version 4.4*.

Davidson, S. M., Andersen, M. B. & Mani, A. 2014 Chaotic induced-charge electro-osmosis. *Phys. Rev. Lett.* **112**, 128302.

Demekhin, E. A., Nikitin, N. V. & Shelistov, V. S. 2013 Direct numerical simulation of electrokinetic instability and transition to chaotic motion. *Phys. Fluids* **25**, 122001.

Demekhin, E. A., Shelistov, V. S. & Polyanskikh, S. V. 2011 Linear and nonlinear evolution and diffusion layer selection in electrokinetic instability. *Phys. Rev. E* **84**, 036318.

Druzgalski, C. L., Andersen, M. B. & Mani, A. 2013 Direct numerical simulation of electroconvective instability and hydrodynamic chaos near an ion-selective surface Introduction. *Phys. Fluids* **25**, 110804.

Fleury, V., Chazalviel, J.-N. & Rosso, M. 1992 Theory and experimental evidence of electroconvection around electrochemical deposits. *Phys. Rev. Lett.* **68**, 2492–2495.

Freitas, C. J. 1995 Perspective: Selected benchmarks from commercial cfd codes. *J. Fluid Eng.* **117**, 208–218.

Glatzel, T., Litterst, C., Cupelli, C., Lindemann, T., Moosmann, C.,

Niekrawietz, R., Streule, W., Zengerle, R. & Koltay, P. 2008 Computational fluid dynamics (CFD) software tools for microfluidic applications-a case study. *Comput. & Fluids* **37**, 218 – 235.

Green, Y., Shlousb, S. & Yossifon, G. 2014 Effect of geometry on concentration polarization in realistic heterogeneous permselective systems. *Phys. Rev. E* **89**, 043015.

Iaccarino, G. 2001 Predictions of a turbulent separated flow using commercial cfd codes. *J. Fluid Eng.* **123**, 819–828.

Kambiz, S. & Patrick, K. 2000 *Code verification by the method of manufactured solutions.* Technical Report no. SAND2000-1444, Sandia National Laboratories.

Kravchenko, A. G. & Moin, P. 2000 Numerical studies of flow over a circular cylinder at Re[sub D]=3900. *Phys. Fluids* **12**, 403.

Krol, J. 1999 Concentration polarization with monopolar ion exchange membranes: current-voltage curves and water dissociation. *J. Membrane Sci.* **162**, 145–154.

Kwak, R., Pham, V. S., Lim, K. M. & Han, J. 2013 Shear flow of an electrically charged fluid by ion concentration polarization: scaling laws for electroconvective vortices. *Phys. Rev. Lett.* **110**, 114501.

Manzanares, J. A., Mafd, S. & Reiss, H. J. 1993 Numerical simulation of the nonequilibrium diffuse double layer in ion-exchange membranes. *J. Phys. Chem.* **97**, 8524–8530.

Matsuura, T., Fane, T., Kwak, R., Guan, G., Peng, W. K. & Han, J. 2013 Microscale electrodialysis: Concentration profiling and vortex visualization. *Desalination* **308**, 138–146.

Mishchuk, N. 2010 Concentration polarization of interface and non-linear electrokinetic phenomena. *Adv. Colloid. Inter. Sci.* **160**, 16–39.

Mittal, R. & Moin, P. 1997 Suitability of upwind-biased finite difference schemes for large-eddy simulation of turbulent flows. *AIAA J.* **35**, 1415–1417.

Nikonenko, V. V., Kovalenko, A. V., Urtenov, M. K., Pismenskaya, N. D., Han, J., Sistat, P. & Pourcelly, G. 2014 Desalination at overlimiting currents: state-of-the-art and perspectives. *Desalination* **342**, 85–106.

Rubinstein, I. & Zaltzman, B. 2000 Electro-osmotically induced convection at a permselective membrane. *Phys. Rev. E* **62**, 2238–2251.

Rubinstein, I. & Zaltzman, B. 2001 Electro-osmotic slip of the second kind and instability in concentration polarization at electrodialysis membranes. *Math. Models Methods App. Sci.* **11**, 263–300.

Tucker, P. 1997 Cfd applied to electronic systems: a review. *IEEE T Compon Pack T* **20**, 518–529.

Yariv, E. 2009 Asymptotic current-voltage relations for currents exceeding the diffusion limit. *Phys. Rev. E* **80**, 051201.

Zangle, T. A., Mani, A. & Santiago, J. G. 2010 Theory and experiments of concentration polarization and ion focusing at microchannel and nanochannel interfaces. *Chem. Soc. Rev.* **39**, 1014–35.